SCIENTIFIC REPORTS

Universal Conductance Fluctuation in Two-Dimensional Topological Insulators

Duk-Hyun Choe & K. J. Chang

Despite considerable interest in two-dimensional (2D) topological insulators (TIs), a fundamental question still remains open how mesoscopic conductance fluctuations in 2D TIs are affected by spin-orbit interaction (SOI). Here, we investigate the effect of SOI on the universal conductance fluctuation (UCF) in disordered 2D TIs. Although 2D TI exhibits UCF like any metallic systems, the amplitude of these fluctuations is distinguished from that of conventional spin-orbit coupled 2D materials. Especially, in 2D systems with mirror symmetry, spin-flip scattering is forbidden even in the presence of strong intrinsic SOI, hence increasing the amplitude of the UCF by a factor of $\sqrt{2}$ compared with extrinsic SOI that breaks mirror symmetry. We propose an easy way to experimentally observe the existence of such spin-flip scattering in 2D materials. Our findings provide a key to understanding the emergence of a new universal behavior in 2D TIs.

Quantum interference of electrons in mesoscopic systems leads to the striking transport phenomena, the so-called universal conductance fluctuations (UCF)[1]. It predicts that disordered mesoscopic systems with sizes smaller than the phase coherent length exhibit sample-to-sample conductance fluctuations in the order of e^2/h, independent of the details of the system such as material properties, disorder strength, and sample size. The UCF only depends the dimensionality and universality class of the system, as can be understood in the framework of the random matrix theory[2,3]. Time reversal symmetry (TRS) and spin rotational symmetry (SRS) play an important role in determining the universality class. There exist three types of universality classes: circular orthogonal ensemble ($\beta = 1$), where TRS and SRS are present; circular unitary ensemble ($\beta = 2$), where TRS is broken; circular symplectic ensemble ($\beta = 4$), where SRS is broken and TRS is preserved.

Recent discoveries of novel two-dimensional (2D) materials[4] have raised several interesting issues in the quantum interference effects such as weak (anti)localization[5,6] and UCF[7–13]. In particular, graphene exhibits unusual UCF behavior. When disorder is governed by long-range potentials, the inter-valley scattering of Dirac fermions is suppressed in graphene, hence the amplitude of the UCF is increased by a factor of 2 compared with conventional metals[7–9]. Moreover, it was suggested that the finite size effects in graphene can lead to a systematic deviation from the universal behavior[10]. More importantly, in the presence of strong spin-orbit interaction (SOI) in graphene, Qiao and coworkers[11] have shown that the universal spin Hall conductance fluctuation, an analogue of the UCF in spin Hall conductance[12,13], does not follow the conventional value for the circular symplectic ensemble of $\beta = 4$. Although it was argued that a new type of universality class exists, its origin is not clearly resolved.

Strong SOIs in 2D systems, on the other hand, give rise to a wide range of intriguing physical phenomena such as spin-valley coupling[14,15] and quantum spin Hall effect[16–18]. Quantum spin Hall insulators, i.e., 2D topological insulators (TIs)[19–24], have bulk insulating gaps as well as conducting edge states that are topologically protected against backscattering by TRS. Kane and Mele have derived the formula for SOI in graphene[16] by taking into account allowed symmetries in the lattice, where the intrinsic SOI opens a nontrivial energy gap near the Dirac point. Although the SOI in pristine graphene is weak[25], a number of strategies have been proposed to enhance the coupling strength, for instance, by hydrogenation[26–28],

Department of Physics, Korea Advanced Institute of Science and Technology, Daejeon 305-701, Rep. of Korea. Correspondence and requests for materials should be addressed to K.J.C. (email: kjchang@kaist.ac.kr)

adsorption of transition metal adatoms[29–32], and proximity-induced effects[33–38]. Very recently, it was predicted that strong intrinsic SOI in 2D transition metal dichalcogenides leads to a quantum spin Hall phase[24], and a SOI-induced band gap opening was experimentally observed in $MoTe_2$ with a distorted octahedral structure[39]. Due to the growing interest in 2D TIs, the role of SOI in the band topology has become quite well established. However, a fundamental question that has remained open is how mesoscopic conductance fluctuations in 2D TIs are affected by SOI. Characterizing the nature of mesoscopic conductance fluctuation is important for understanding quantum interference of the electrons in 2D TIs.

Here, we report a comprehensive analysis of the conductance fluctuation behavior in 2D TIs in the presence of short-range disorders. As a representative example, we consider the graphene TI system where intrinsic and extrinsic SOIs are described by the Kane-Mele (KM) and Rashba models, respectively. We demonstrate that, although graphene TI shows *universal* conductance fluctuations like any metallic systems, the amplitude of these fluctuations is distinguished from that of conventional spin-orbit coupled 2D materials. Thereby, we establish a theoretical framework for interpreting the peculiar conductance fluctuations in 2D TIs by clarifying the role of underlying symmetries of the system. We further elucidate the combined effect of SOI and symmetry breaking magnetic field on the UCF.

Methods

Disordered graphene with SOI is described by a tight-binding (TB) Hamiltonian, $H = H_g + H_{SO} + H_{disorder}$. The first term represents the usual nearest-neighbor interaction, $H_g = -\sum_{\langle i,j\rangle} t_{ij} e^{i\phi_{ij}} c_i^\dagger c_j$, where c_i ($c_i^\dagger$) is the annihilation (creation) operator on the ith lattice site. The effect of TRS breaking by an external magnetic field B is taken into account by introducing the magnetic flux, $\phi_{ij} = \frac{e}{\hbar}\int_{r_i}^{r_j} \mathbf{A} \cdot dl$, where $\mathbf{A} = (-By, 0, 0)$ is the vector potential, but the Zeeman splitting is neglected. The intrinsic and extrinsic SOIs are described by KM and Rashba terms, respectively, as follows[16,17]:

$$H_{SO} = H_{KM} + H_R = -i\lambda_{KM}\sum_{\langle\langle i,j\rangle\rangle} e^{i\phi_{ij}}\left(\hat{\mathbf{d}}_{in} \times \hat{\mathbf{d}}_{jn}\right)_z c_i^\dagger s^z c_j - i\lambda_R\sum_{\langle i,j\rangle} e^{i\phi_{ij}} c_i^\dagger\left(\mathbf{s} \times \hat{\mathbf{d}}_{ij}\right)_z c_j, \tag{1}$$

where $\langle\ldots\rangle$ and $\langle\langle\ldots\rangle\rangle$ denote the nearest-neighbor and next-nearest-neighbor interactions, respectively, and s^z is a Pauli matrix representing the electron spin.

Short-range disorders are introduced by adding random on-site energies or adatoms,

$$H_{disorder} = H_{Anderson} + H_{adatom} = \sum_i \varepsilon_i c_i^\dagger c_i - \sum_n \gamma_{ad}(c_{p_n}^\dagger d_n + c_{p_n} d_n^\dagger). \tag{2}$$

Here ε_i is randomly chosen in the range ($-W/2 < \varepsilon_i < W/2$), with the disorder strength W, d_n ($d_n^\dagger$) is the annihilation (creation) operator on the nth adatom site, and p_n is the host site bonded to the adatom. The hopping integrals are determined by fitting the band structure to that of density functional calculations[40,41], such as $t_{ij} = 2.6$ between the C atoms in pristine graphene, $t_{ij} = 3.2$ between the edge C atoms, and $\gamma_{ad} = 5.72$ between the host C atom and adatom in the case of H adatoms with concentrations n_{ad}. Other type of adatoms should give qualitatively similar results except for the breaking of electron-hole symmetry[42]. The adatom-induced SOI[26,28] is not included.

For a device model in which a disordered graphene nanoribbon (GNR) of 100 nm length is sandwiched between two semi-infinite GNR electrodes, the two-terminal conductance is calculated by using the Landauer-Büttiker formula, $G = (e^2/h)Tr(tt^\dagger)$, where t is the transmission matrix. To examine the sample-to-sample fluctuation behavior in the conductance of the system, we analyze the data statistically. Individual data points are obtained by taking the ensemble average over more than 2,000 different configurations.

Results and Discussion

We first discuss the effect of the intrinsic SOI (H_{KM}) on the electronic structure of pristine systems in Fig. 1. To identify the one-dimensional edge state, we consider two armchair graphene nanoribbons (N-aGNRs) of about 10 nm width, where N is the number of C-C dimer lines across the ribbon. For 83-aGNR and 82-aGNR, the bulk band gaps are 0.04 and 0.15 eV, respectively. In the strong coupling regime ($\lambda_{KM} = 0.1$, $\lambda_R = 0$), the band gaps of both aGNRs increase to 0.95 eV due to the SOI, and the topological edge states appear in the gaps [Fig. 1(a,b)]. When periodic boundary conditions (PBC) are imposed along the transverse direction in 82-aGNR, the edge states are removed whereas the bulk gap remains unchanged [Fig. 1(c)].

To understand the influence of disorder on the transport properties of graphene TI, we plot the averaged conductance of disordered GNRs as a function of channel energy for $\lambda_{KM} = 0.1$ in Fig. 2(a). For moderate strengths of Anderson disorder ($W = 1.5, 2.0$), the edge states ($E > -0.5$ eV) are unaffected by the disorder and hence the electron transport is ballistic, indicating the robustness of the topological edge states[22]. In the case of adatom disorder, however, the edge states become slightly damaged close to the neutrality point due to the formation of strongly localized adatom defect states[40]. Despite this, most of the states are still in the (quasi-)ballistic transport regime. If we remove the edge states by imposing PBC, the conductance value drops to zero [dotted lines in Fig. 2(a)]. On the other hand, for the bulk states
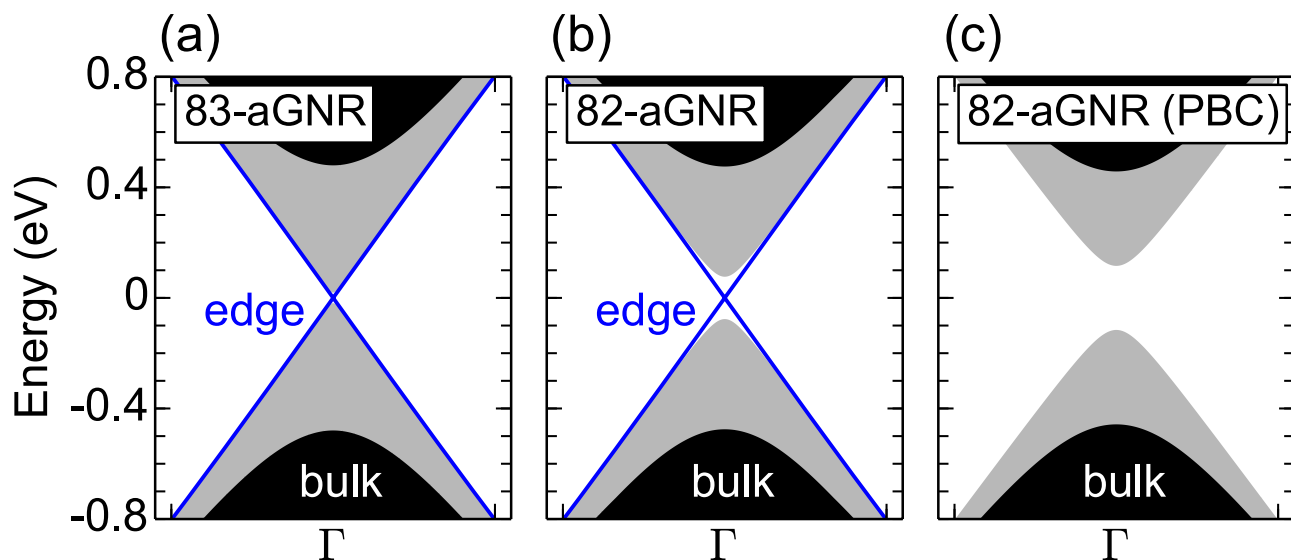
Figure 1. Band structures of graphene TIs. Band structures of (**a**) 83-aGNR, (**b**) 82-aGNR, and (**c**) 82-aGNR with periodic boundary conditions in the presence of intrinsic spin-orbit coupling ($\lambda_{KM} = 0.1$). The bulk and edge states are illustrated as black regions and blue lines, respectively. For comparison, the bulks states of pristine aGNRs for $\lambda_{KM} = 0$ are illustrated as gray shaded regions.
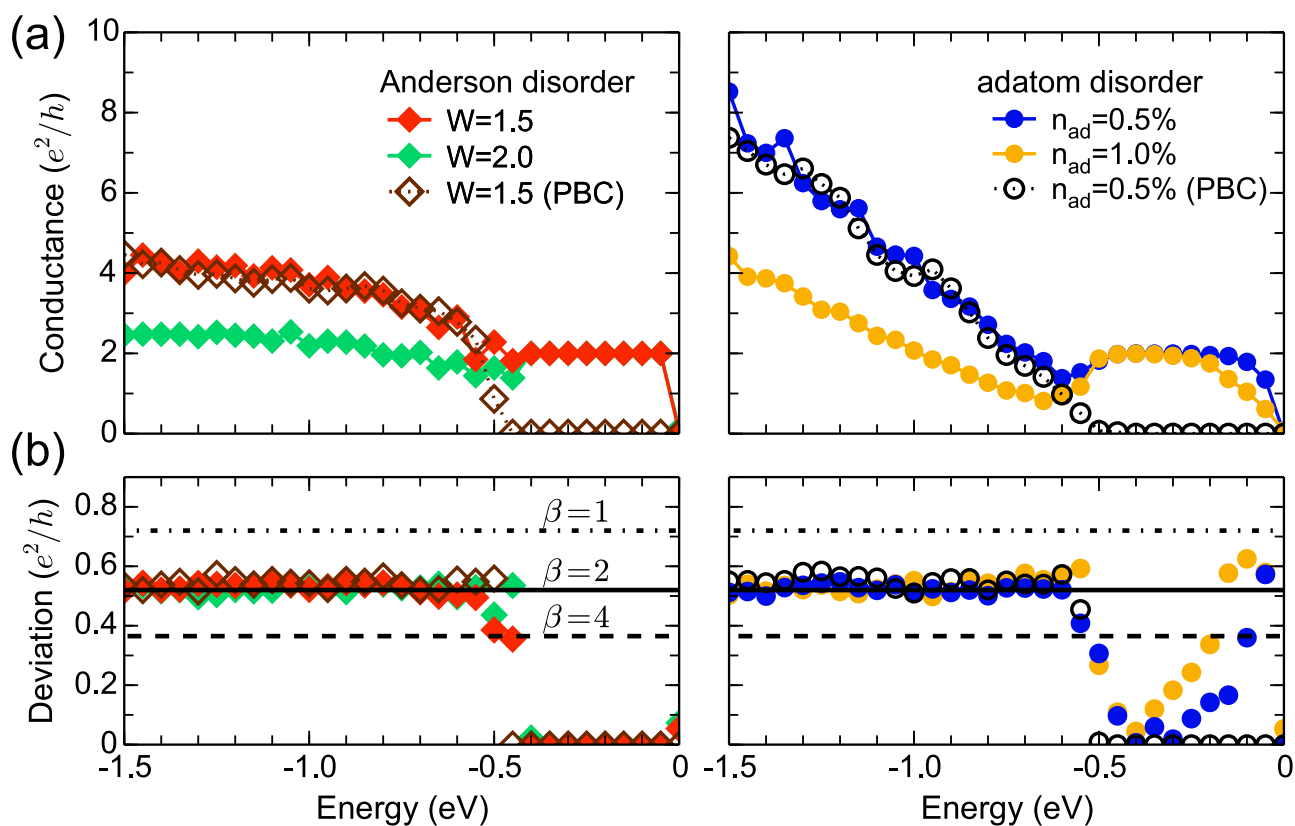
Figure 2. Electronic transport characteristics. (**a**) Averaged conductance and (**b**) its deviation values are plotted as a function of channel energy for 83-aGNRs of 100 nm length in the presence of Anderson and adatom disorders. For comparison, the results are also given for 82-aGNRs with periodic boundary conditions (empty symbols). The lines in (**b**) represent the deviation values predicted by the UCF theory for circular orthogonal ensembles ($\beta = 1$), circular unitary ensembles ($\beta = 2$), and circular symplectic ensembles ($\beta = 4$) in quasi-one-dimensional systems[1,2].

($E < -0.5\,$eV) in the diffusive regime, conductance is suppressed and exhibits large sample-to-sample fluctuations depending on the disorder strength.

Graphene-based TI, like any metallic or semiconducting systems, exhibits *universal* conductance fluctuations when the electron transport is diffusive. However, the amplitude of these fluctuations is distinguished from that of previously studied spin-orbit coupled 2D systems. Figure 2(b) shows the deviation of conductance as a function of channel energy in 83-aGNR and 82-aGNR. Since the edge states are robust against the disorder, conductance fluctuations are mostly zero for energies above $-0.5\,$eV. The conductance fluctuation in the case of adatom disorder is associated with the hopping between defect states[40]. In the diffusive transport regime below $-0.5\,$eV, regardless of the channel energy, disorder type, and disorder strength, the conductance fluctuation exhibits the universal behavior with the UCF value of $0.52\,e^2/h$. Note that this UCF value corresponds to that estimated from the circular unitary ensemble ($\beta = 2$), and differs from the estimated value of $0.365\,e^2/h$ for the Rashba SOI ($\beta = 4$)[1,43,44], although H_{KM} breaks the SRS and preserves the TRS. Such a discrepancy is not originated from the topological edge states because the UCF is independent of the PBC, as shown in Fig. 2(b).

The distinct UCF value in the KM model is attributed to the particular form of H_{KM}, which lacks the spin-flip term. H_{KM} consists of two Haldane Hamiltonians ($H_{Haldane}$) for up and down spins. In the Haldane model[45,46], periodic magnetic flux densities are introduced, while the total flux is zero within the unit cell. The Haldane model is categorized as the circular unitary ensemble ($\beta = 2$) since the phase acquired by the next-nearest-neighbor hopping term breaks the TRS. The general form of $H_{Haldane}$ is $H_{Haldane} = - i\lambda_H \sum_{\langle\langle i,j \rangle\rangle} \left(\hat{\mathbf{d}}_{in} \times \hat{\mathbf{d}}_{jn} \right)_z c_i^\dagger c_j$, where λ_H is the coupling constant. Therefore, including s^z and substituting λ_H for λ_{KM} in $H_{Haldane}$ exactly result in the KM Hamiltonian [Eq. (1)]. Due to the s^z term, H_{KM} preserves the TRS and its system belongs to the circular symplectic ensemble ($\beta = 4$). That is to say, the combination of two $\beta = 2$ ensembles results in the $\beta = 4$ ensemble. Since H_{KM} is just a direct sum of spin-up and spin-down Haldane terms with each component having the opposite sign, $H_{KM} = H_{Haldane}^+ \oplus H_{Haldane}^-$, the conductance values obtained by H_{KM} are identical to those of $H_{Haldane}$. As a result, the intrinsic SOI in graphene TI (H_{KM}) leads to the exactly the same UCF value as that derived from $H_{Haldane}$, which is larger by a factor of $\sqrt{2}$ compared with the extrinsic SOI case (H_R) [Fig. 3(b)].

Here, we emphasize that our analysis for the graphene KM model can be extended to generic 2D systems. The microscopic SOI is described by the Hamiltonian of $H_{SO} \sim \mathbf{s} \cdot (\nabla V \times \mathbf{p})$. When (1) electrons are confined in 2D systems ($p = p_x \hat{\mathbf{i}} + p_y \hat{\mathbf{j}}$) and (2) the mirror symmetry with respect to the 2D plane is present ($\partial V/\partial z = 0$), the allowed interaction is given by $s^z(\partial V/\partial x p_y - \partial V/\partial y p_x)$. Due to the s^z-related term, the spin-flip scattering does not take place, indicating that spin-up and spin-down states are well separated. Furthermore, spin-up and spin-down components are identical except for the sign as in the KM model [Eq. (1)]. These results imply that, when 2D materials have both the intrinsic SOI and the mirror symmetry about the plane, the same UCF behavior as that of the KM model should be observed. A more fundamental origin of such a distinct UCF value in graphene-based TI, therefore, is the perfect 2D nature of graphene and the intrinsic SOI that preserves the mirror symmetry.

We compare the effects of an external magnetic field B, $H_{Haldane}$, H_{KM}, and H_R on the UCF behavior in Fig. 3. When only an external magnetic field is applied perpendicular to the 2D plane, the universality class changes from a circular orthogonal ensemble ($\beta = 1$) to a circular unitary ensemble ($\beta = 2$). The gradual evolution of the UCF value from 0.72 to $0.52\,e^2/h$ with increasing of B is independent of the type and strength of disorders [Fig. 3(a)]. The reduced UCF value by a factor of $\sqrt{2}$ is attributed to the elimination of the particle-particle channels (so-called Cooperons), according to the diagrammatic perturbation theory[1].

For $B = 0$, all the UCF values converge to $0.52\,e^2/h$ for the KM and Haldane interactions [Fig. 3(b)], following the trend of the B field only. The calculated conductance and its deviation values are exactly the same for the KM and Haldane interactions, due to the underlying symmetries of the Hamiltonians as discussed earlier. It is clear again that the existence of the topological edge states does not affect the UCF behavior [dashed lines in Fig. 3(b)]. On the other hand, when the Rashba SOI involving spin-flip scattering is considered, where the SOI breaks both SRS and the mirror symmetry, the UCF value is reduced by a factor of 2 as expected[1,2,43,44].

To illustrate the difference between the Haldane and KM interactions, we now turn on the magnetic field in such systems. For a magnetic field of $B = 50\,$T, the UCF values are plotted as a function of interaction parameters (λ_H, λ_{KM}, and λ_R) in Fig. 3(c). In the Haldane interaction, since TRS is already broken, increasing the magnetic field does not change the universality class, thus, the UCF value remains unchanged. In the KM interaction, the magnetic field reduces the UCF value by a factor of $\sqrt{2}$, in contrast to the case of $B = 0$ [Fig. 3(b)]. The reduced UCF value is attributed to different symmetries in the two interactions: the magnetic field breaks the symmetry between up and down spins in H_{KM}, while $H_{Haldane}$ maintains the spin symmetry even for $B \neq 0$. In the Rashba interaction, the magnetic field further decreases the UCF value from 0.365 to $0.258\,e^2/h$ (by a factor of $\sqrt{2}$)[47].

We examine the combined effect of KM and Rashba interactions on the deviation of conductance. We choose the Rashba coupling of $\lambda_R = 0.15$ to ensure that the system is initially in the circular symplectic ensemble ($\beta = 4$). For $B = 0$, as the KM coupling λ_{KM} increases from 0 to 0.2, the UCF does not change
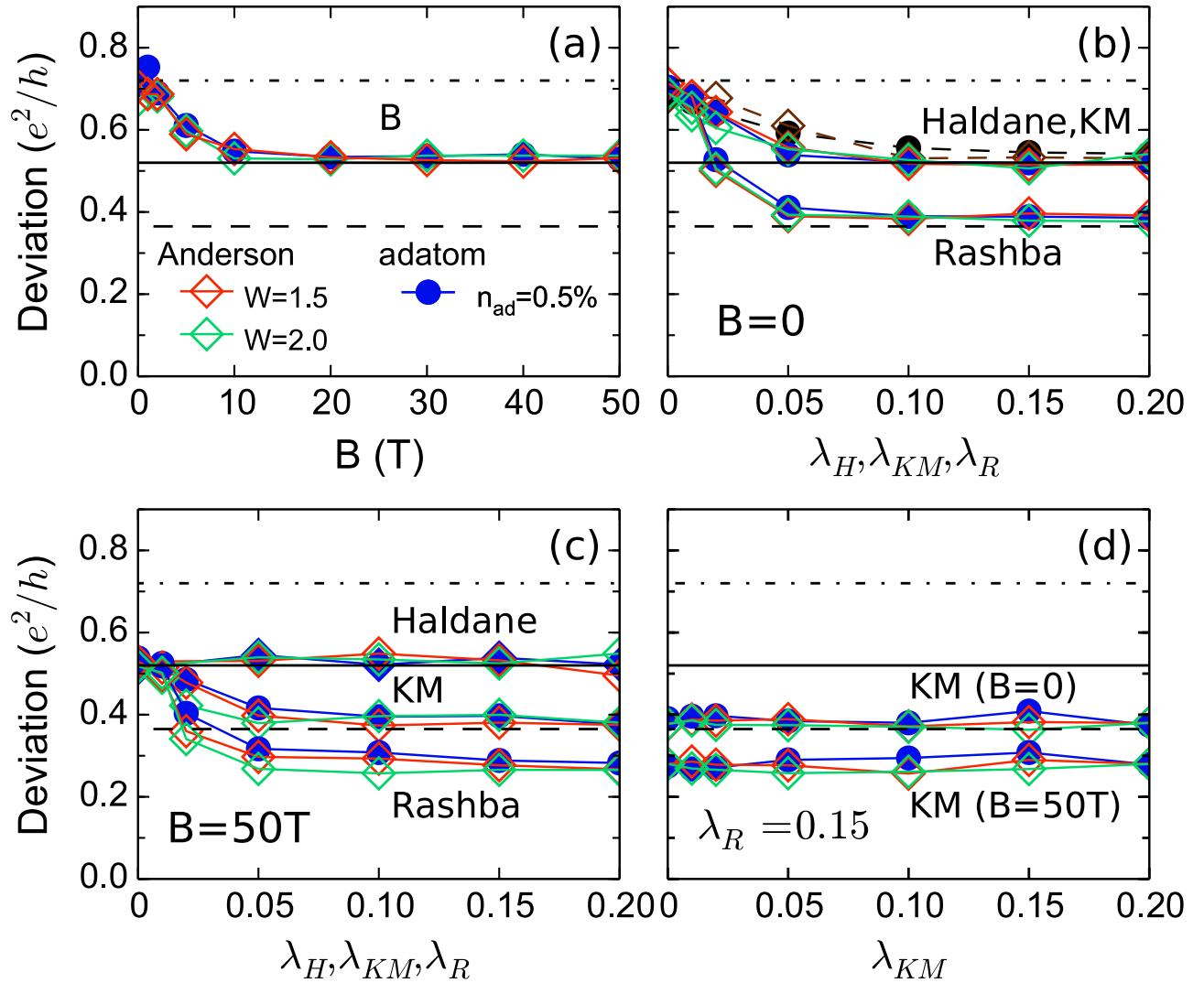
Figure 3. The UCF in the presence of various interactions. Black dotted, solid, and dashed lines denote the predicted UCF values for $\beta = 1$, $\beta = 2$, and $\beta = 4$, respectively, as in Fig. 2(b). Red, green, and blue symbols represents the calculated deviation values for disorder strengths of $W = 1.5$, $W = 2.0$, and $n_{ad} = 0.5\%$, respectively. Channel energy is set to $-1.2\,eV$. (**a**) Deviations as a function of an external magnetic field (B) for $\lambda_{KM} = \lambda_H = \lambda_R = 0$, (**b**)-(**c**) deviations as a function of λ_H, λ_{KM}, and λ_R for $B = 0$ and 50 T, and (**d**) deviations as a function of λ_{KM} in the presence of Rashba coupling ($\lambda_R = 0.15$) for $B = 0$ and 50 T. In (**b**), two dashed lines denote the results for 82-aGNRs with periodic boundary conditions.

with the value of $0.365\,e^2/h$, implying that the system maintains the universality class of $\beta = 4$. When a magnetic field of 50 T is additionally applied, the UCF value is reduced to $0.258\,e^2/h$ for all the values of λ_{KM}, similar to the Rashba case in Fig. 3(c). The UCF behavior, therefore, is not influenced by the intrinsic SOI as long as the extrinsic SOI involving spin-flip scattering is present in the system.

In graphene, it may be difficult to realize a spin-orbit coupled system without spin-flip scattering, because enhancing the SOI generally involves the breaking of mirror symmetry which leads to the Rashba-type interaction[26–33]. However, graphene TIs in sandwiched structures[35,36] and monolayer transition metal dichalcogenides in trigonal prismatic (1H) structure[14,15] can provide a promising platform for testing our prediction, because they have both strong SOI and mirror symmetry. In such systems, increasing the Rashba coupling by applying an external electric field would lead to the $1/\sqrt{2}$ reduction of the UCF value, as illustrated in Fig. 3(d), instead of the $1/2$ reduction in Fig. 3(b). On the other hand, if spin-flip scattering initially exists in the system, an electric field will not affect the UCF behavior. Therefore, the $1/\sqrt{2}$ reduction of the UCF value by applying an electric field could serve as a signature reflecting the absence of spin-flip scattering in 2D materials. In graphene devices[17,26], the electric-field-induced Rashba coupling was predicted to be extremely small (about $10^{-8} \sim 10^{-5}\,eV$)

presumably due to neglecting the effect of orbital angular momentum[48]. However, a substantial Rashba splitting up to 0.1 eV was observed[49] when Au atoms were intercalated between graphene and substrate.

As a final remark, our understanding of the UCF behavior in spin-orbit coupled systems would enable us to reveal the exotic spin Hall conductance fluctuations predicted in 2D TIs. It was reported that, in 2D materials such as graphene and HgTe quantum well, the intrinsic SOI leads to an amplitude of the universal spin Hall conductance fluctuation ($= 0.285\, e/4\pi$)[11,50], which is larger than that of the extrinsic (Rashba-type) SOI ($= 0.18\, e/4\pi$)[11–13], similar to the UCF case. The reason for this discrepancy remains to be clarified. Although the arguments in our study for charge transport cannot be directly used to explain the spin Hall conductance behavior, our results provide important insights to understanding the role of intrinsic and extrinsic SOIs in 2D systems.

In conclusion, we have shown that the underlying symmetries of the system, rather than the topological edge states, play a key role in characterizing the UCF in 2D TIs. In 2D materials with both strong SOI and mirror symmetry, we find that the UCF value can be reduced by a factor of $\sqrt{2}$ by applying an external electric field, while it is not affected when mirror symmetry is initially broken. Thus, our findings can be experimentally confirmed by observing the effect of an electric field on the UCF, which reflects the existence of spin-flip scattering in 2D materials.

References

1. Lee, P. & Stone, A. Universal Conductance Fluctuations in Metals. *Phys. Rev. Lett.* **55,** 1622–1625 (1985).
2. Beenakker, C. Random-matrix theory of quantum transport. *Rev. Mod. Phys.* **69,** 731–808 (1997).
3. Aleiner, I. & Fal'ko, V. Spin-Orbit Coupling Effects on Quantum Transport in Lateral Semiconductor Dots. *Phys. Rev. Lett.* **87,** 256801 (2001).
4. Castro Neto, A. H., Peres, N. M. R., Novoselov, K. S. & Geim, A. K. The electronic properties of graphene. *Rev. Mod. Phys.* **81,** 109–162 (2009).
5. McCann, E. *et al.* Weak-Localization Magnetoresistance and Valley Symmetry in Graphene. *Phys. Rev. Lett.* **97,** 146805 (2006).
6. Shan, W.-Y., Lu, H.-Z. & Shen, S.-Q. Spin-orbit scattering in quantum diffusion of massive Dirac fermions. *Phys. Rev. B* **86,** 125303 (2012).
7. Kechedzhi, K., Kashuba, O. & Fal'ko, V. Quantum kinetic equation and universal conductance fluctuations in graphene. *Phys. Rev. B* **77,** 193403 (2008).
8. Kharitonov, M. & Efetov, K. Universal conductance fluctuations in graphene. *Phys. Rev. B* **78,** 033404 (2008).
9. Pal, A. N., Kochat, V. & Ghosh, A. Direct Observation of Valley Hybridization and Universal Symmetry of Graphene with Mesoscopic Conductance Fluctuations. *Phys. Rev. Lett.* **109,** 196601 (2012).
10. Rossi, E., Bardarson, J., Fuhrer, M. & Das Sarma, S. Universal Conductance Fluctuations in Dirac Materials in the Presence of Long-range Disorder. *Phys. Rev. Lett.* **109,** 096801 (2012).
11. Qiao, Z., Wang, J., Wei, Y. & Guo, H. Universal Quantized Spin-Hall Conductance Fluctuation in Graphene. *Phys. Rev. Lett.* **101,** 016804 (2008).
12. Ren, W., Qiao, Z., Wang, J., Sun, Q. & Guo, H. Universal Spin-Hall Conductance Fluctuations in Two Dimensions. *Phys. Rev. Lett.* **97,** 066603 (2006).
13. Bardarson, J., Adagideli, İ. & Jacquod, P. Mesoscopic Spin Hall Effect. *Phys. Rev. Lett.* **98,** 196601 (2007).
14. Xiao, D., Liu, G.-B., Feng, W., Xu, X. & Yao, W. Coupled Spin and Valley Physics in Monolayers of MoS$_2$ and Other Group-VI Dichalcogenides. *Phys. Rev. Lett.* **108,** 196802 (2012).
15. Chhowalla, M. *et al.* The chemistry of two-dimensional layered transition metal dichalcogenide nanosheets. *Nature Chem.* **5,** 263–275 (2013).
16. Kane, C. L. & Mele, E. J. Quantum Spin Hall Effect in Graphene. *Phys. Rev. Lett.* **95,** 226801 (2005).
17. Kane, C. L. & Mele, E. J. Z$_2$ Topological Order and the Quantum Spin Hall Effect. *Phys. Rev. Lett.* **95,** 146802 (2005).
18. Bernevig, B. A. & Zhang, S.-C. Quantum Spin Hall Effect. *Phys. Rev. Lett.* **96,** 106802 (2006).
19. Bernevig, B. A., Hughes, T. L. & Zhang, S.-C. Quantum spin Hall effect and topological phase transition in HgTe quantum wells. *Science* **314,** 1757–1761 (2006).
20. König, M. *et al.* Quantum spin hall insulator state in HgTe quantum wells. *Science* **318,** 766–770 (2007).
21. Liu, C., Hughes, T., Qi, X.-L., Wang, K. & Zhang, S.-C. Quantum Spin Hall Effect in Inverted Type-II Semiconductors. *Phys. Rev. Lett.* **100,** 236601 (2008).
22. Hasan, M. Z. & Kane, C. L. Colloquium: Topological insulators. *Rev. Mod. Phys.* **82,** 3045–3067 (2010).
23. Xu, Y. *et al.* Large-Gap Quantum Spin Hall Insulators in Tin Films. *Phys. Rev. Lett.* **111,** 136804 (2013).
24. Qian, X., Liu, J., Fu, L. & Li, J. Quantum spin Hall effect in two-dimensional transition metal dichalcogenides. *Science* **346,** 1344–1347 (2014).
25. Min, H. *et al.* Intrinsic and Rashba spin-orbit interactions in graphene sheets. *Phys. Rev. B* **74,** 165310 (2006).
26. Castro Neto, A. H. & Guinea, F. Impurity-Induced Spin-Orbit Coupling in Graphene. *Phys. Rev. Lett.* **103,** 026804 (2009).
27. Balakrishnan, J., Koon Wai Koon, G., Jaiswal, M., Castro Neto, A. H. & Özyilmaz, B. Colossal enhancement of spin–orbit coupling in weakly hydrogenated graphene. *Nature Phys.* **9,** 284–287 (2013).
28. Gmitra, M., Kochan, D. & Fabian, J. Spin-Orbit Coupling in Hydrogenated Graphene. *Phys. Rev. Lett.* **110,** 246602 (2013).
29. Weeks, C., Hu, J., Alicea, J., Franz, M. & Wu, R. Engineering a Robust Quantum Spin Hall State in Graphene via Adatom Deposition. *Phys. Rev. X* **1,** 021001 (2011).
30. Hu, J., Alicea, J., Wu, R. & Franz, M. Giant Topological Insulator Gap in Graphene with 5d Adatoms. *Phys. Rev. Lett.* **109,** 266801 (2012).
31. Jiang, H., Qiao, Z., Liu, H., Shi, J. & Niu, Q. Stabilizing Topological Phases in Graphene via Random Adsorption. *Phys. Rev. Lett.* **109,** 116803 (2012).
32. Autès, G. & Yazyev, O. V. Engineering quantum spin Hall effect in graphene nanoribbons via edge functionalization. *Phys. Rev. B* **87,** 241404 (2013).
33. Jin, K.-H. & Jhi, S.-H. Proximity-induced giant spin-orbit interaction in epitaxial graphene on a topological insulator. *Phys. Rev. B* **87,** 075442 (2013).
34. Li, Y. *et al.* Topological insulators in transition-metal intercalated graphene: The role of d electrons in significantly increasing the spin-orbit gap. *Phys. Rev. B* **87,** 245127 (2013).
35. Kou, L. *et al.* Graphene-based topological insulator with an intrinsic bulk band gap above room temperature. *Nano Lett.* **13,** 6251–6255 (2013).
36. Kou, L. *et al.* Robust 2D topological insulators in van der Waals heterostructures. *ACS Nano* **8,** 10448–10454 (2014).

37. Popov, I., Mantega, M., Narayan, A. & Sanvito, S. Proximity-induced topological state in graphene. *Phys. Rev. B* **90,** 035418 (2014).
38. Calleja, F. *et al.* Spatial variation of a giant spin–orbit effect induces electron confinement in graphene on Pb islands. *Nature Phys.* **11,** 43– 47 (2014).
39. Keum, D. *et al.* Bandgap opening in few-layered monoclinic $MoTe_2$. *Nature Phys.* in production doi:10.1038/nphys3314 (2015).
40. Choe, D.-H., Bang, J. & Chang, K. J. Electronic structure and transport properties of hydrogenated graphene and graphene nanoribbons. *New J. Phys.* **12,** 125005 (2010).
41. Choe, D.-H. & Chang, K. J. Effect of dimensionality on the localization behavior in hydrogenated graphene systems. *Nano Lett.* **12,** 5175–5180 (2012).
42. Wehling, T. O., Yuan, S., Lichtenstein, A. I., Geim, A. K. & Katsnelson, M. I. Resonant Scattering by Realistic Impurities in Graphene. *Phys. Rev. Lett.* **105,** 056802 (2010).
43. Qiao, Z., Xing, Y. & Wang, J. Universal conductance fluctuation of mesoscopic systems in the metal-insulator crossover regime. *Phys. Rev. B* **81,** 085114 (2010).
44. Takagaki, Y. Conductance fluctuations induced by bulk state in quasi-one-dimensional strips of topological insulator. *Phys. Rev. B* **85,** 155308 (2012).
45. Haldane, F. D. M. Model for a Quantum Hall Effect without Landau Levels: Condensed-Matter Realization of the "Parity Anomaly." *Phys. Rev. Lett.* **61,** 2015–2018 (1988).
46. Jotzu, G. *et al.* Experimental realization of the topological Haldane model with ultracold fermions. *Nature* **515,** 237–240 (2014).
47. Feng, S. Mesoscopic conductance fluctuations in the presence of spin-orbit coupling and Zeeman splitting. *Phys. Rev. B* **39,** 8722–8724 (1989).
48. Park, S. R., Kim, C. H., Yu, J., Han, J. H. & Kim, C. Orbital-Angular-Momentum Based Origin of Rashba-Type Surface Band Splitting. *Phys. Rev. Lett.* **107,** 156803 (2011).
49. Marchenko, D. *et al.* Giant Rashba splitting in graphene due to hybridization with gold. *Nat. Commun.* **3,** 1232 (2012).
50. Qiao, Z., Ren, W. & Wang, J. Universal Spin-Hall Conductance Fluctuations in Two-Dimensional Mesoscopic Systems. *Mod. Phys. Lett. B* **25,** 359–376 (2011).

Acknowledgment

Author Contributions

D.-H.C. carried out the calculations. K.J.C. assisted the data analysis. D.-H.C. and K.J.C. discussed the results and wrote the manuscript.

Additional Information

Competing financial interests: The authors declare no competing financial interests.

How to cite this article: Choe, D.-H. and Chang, K. J. Universal Conductance Fluctuation In Two-Dimensional Topological Insulators. *Sci. Rep.* **5**, 10997; doi: 10.1038/srep10997 (2015).